34th Annual International Conference of the IEEE EMBS
San Diego, California USA, 28 August - 1 September, 2012

CAUSAL MARKOV RANDOM FIELD FOR BRAIN MR IMAGE SEGMENTATION

Qolamreza R. Razlighi[1], Member, IEEE, Aleksey Orekhov, Andrew Laine[2], Fellow, IEEE, Yaakov Stern[1]

[1]Cognitive Neuroscience Division, Neurology Department, Columbia University
[2]Biomedical Engineering Department, Columbia University

ABSTRACT

We propose a new Bayesian classifier, based on the recently introduced causal Markov random field (MRF) model, Quadrilateral MRF (QMRF). We use a second order inhomogeneous anisotropic QMRF to model the prior and likelihood probabilities in the maximum *a posteriori* (MAP) classifier, named here as MAP-QMRF. The joint distribution of QMRF is given in terms of the product of two dimensional clique distributions existing in its neighboring structure. 20 manually labeled human brain MR images are used to train and assess the MAP-QMRF classifier using the jackknife validation method. Comparing the results of the proposed classifier and FreeSurfer on the Dice overlap measure shows an average gain of 1.8%. We have performed a power analysis to demonstrate that this increase in segmentation accuracy substantially reduces the number of samples required to detect a 5% change in volume of a brain region.

Index Terms— MRF, Causal MRF, Quadrilateral MRF, MRI, brain image segmentation

1. INTRODUCTION

Brain neurodegenerative disorders such as Alzheimer's disease, schizophrenia, and multiple sclerosis are known to be correlated with deviations in neuroanatomical structures of the brain. The ability to quantify these changes in brain morphometry, particularly in longitudinal studies, depends heavily on the accuracy and reproducibility of the brain volumetric segmentation algorithm employed. The limited accuracy of existing brain MR image segmentation methods and the tedious, inconsistent, and time-consuming process of manual labeling makes automating segmentation one of the most fundamental problems in neuroimaging.

Many methods have been proposed for fully automatic segmentation. However, the large number of artifacts in MR images makes automatic segmentation a very difficult task. For instance, the low contrast of boundaries between brain regions can easily cause segmentation methods like region growing and active contours to fail drastically.

The maximum *a posteriori* (MAP) classifier is a probabilistic method for brain MR image segmentation that is used in three of the most prominent neuroimaging software packages (FSL [1], SPM [2], and FreeSurfer [3]). In MAP classifiers, if the prior probability is obtained based on the Markov random field (MRF) model, the method is referred to as MAP-MRF (used in FSL and FreeSurfer) [4]. It has the capacity to label a voxel based on its 1) intensity, 2) location, and 3) the labels assigned to its neighbors. The MAP-MRF framework does not take into account the intensities of neighboring voxels, which is an important piece of information used by a neuroanatomist when doing manual labeling.

Integrating the above four sources of information into the segmentation problem significantly increases its dimensionality/complexity. In order to make this high-dimensional problem tractable, all of the standard neuroimaging software packages make substandard assumptions, in which some of those four sources of information are discarded. These assumptions reduce the segmentation accuracy. Our proposed MAP-QMRF framework is different because it takes into account all four sources of information for more accurate anatomical segmentation while overcoming the intractability problem. This was not possible until the introduction of the new causal Markov model, called Quadrilateral MRF (QMRF) [5]. In MAP-QMRF the prior and the likelihood probability are both computed by the new QMRF model.

Markovianity is a common tool in dealing with the dimensionality problem. The idea behind Markovianity is that if there is a labeled image with a missing label at one voxel, the information about that voxel's label provided by the rest of the labels in the image is equal to the information given only by its neighboring labels. Mathematically, for a family of random variables $\boldsymbol{L} = \{L_1, L_2, \dots, L_m\}$ defined on a regular lattice S (e.g. digital image), each random variable L_i takes a value l_i from a set of discrete labels $\mathcal{L} = \{1,2,3, \dots, K\}$, and $P(L_i = l_i)$ denotes the probability that a random variable at location i, L_i, takes the value l_i from the label set $\mathcal{L}$ which is abbreviated farther as $P(l_i)$. By extending this notation it is easy to say that $P(L_1 = l_1, L_2 = l_2, \dots, L_m = l_m) = P(l_1, l_2, \dots, l_m) = P(\boldsymbol{l})$ in which $\boldsymbol{l} = \{l_1, l_2, \dots, l_m\}$ is a sample or configuration of the random field $\boldsymbol{L}$ corresponding to the realization of the field. Now, the MRF is defined according to two conditions: $P(\boldsymbol{l}) > 0$ for any configuration of $\boldsymbol{l}$, and $P\left(l_i \middle| \boldsymbol{l}_{\{S-i\}}\right) = P\left(l_i \middle| \boldsymbol{l}_{N_i}\right)$ where $\boldsymbol{l}_{N_i}$ is the configuration of the neighboring random variables at location $i \in S$.

The labeled and intensity images are represented here by two random fields, $\boldsymbol{L}$ and $\boldsymbol{D}$, with different sets of discrete labels $\mathcal{L} = \{1,2,3,\dots,K\}$ and $\mathfrak{D} = \{1,2,\dots,G\}$ respectively. Each label in $\mathcal{L}$ represents different brain structures whereas the labels in $\mathfrak{D}$ represent the intensity values used in the image.

Markov Gibbs equivalence gives a simple closed form function for the MRF distribution $P(\boldsymbol{l}) = Z^{-1} exp(\sum_{c\in\mathbb{C}} V_c(\boldsymbol{l}))$ where the clique potential function $V_c(\boldsymbol{l})$ is an arbitrary function which models the dependency between neighboring random variables. How to choose the form and parameters of the potential function for a proper encoding of constraints is a major topic in MRF modeling [4]. In FSL, the prior probability is modeled by a MRF with a clique potential function $V_c(\boldsymbol{l}) = -\delta(l_i - l_j)$, called the Potts model [1]. FreeSurfer uses an arbitrary clique potential function $V_c(\boldsymbol{l}) = -logP(l_i|\boldsymbol{l}_{N_i})$ for this purpose [3]. It is almost impossible to find an optimal potential function which takes into account all the relationships between the voxels in the intensity and labeled images. Thus, despite the initial progress in the brain image segmentation in FSL and FreeSurfer, the recent evaluation studies [6,7] suggest considerable room for improvement.

2. MAP-QMRF CLASSIFIER

A neuroanatomist's decision to assign a voxel to a specific anatomical region is based on two major factors: his/her existing knowledge of brain anatomy and the information in the image. The same approach is used in Bayesian classifiers where the first factor is considered the prior probability and the second is the likelihood.

$$posteriori \propto likelihod \times prior \quad (1)$$

In the simplest case, the single-voxel-based Bayesian classifier can be formulated as:

$$P(l_i|d_i) \propto P(d_i|l_i) \times P(l_i) \quad (2)$$

where l_i represents the label being examined for the i^{th} voxel in S and d_i represents the intensity at that voxel. Prior, $P(l_i)$, is the probability of different labels taking place at location i which can be obtained from a probabilistic atlas. Likelihood $P(d_i|l_i)$ can be either estimated for every location i or it can be simplified further by assuming the in-class homogeneity and $P(d_i|l_i) = P(\mathcal{d}|\ell)$ for every i. This means that if $d_i = d_j = \mathcal{d}$ for a given region ($l_i = l_j = \ell$), then $P(d_i|l_i) = P(d_j|l_j) = P(\mathcal{d}|\ell)$. In this simple format, the decision for labeling a voxel is made only based on its location and its intensity value whereas the information in the neighboring voxels is discarded. Alternatively, one can consider that the probability of having a given anatomy at a given voxel varies depending on the intensities and anatomies found at the neighboring voxels. The MAP-QMRF framework employs inhomogeneous anisotropic QMRF of order one to incorporate the neighboring voxels' information (intensities and anatomies) into the process of classification. A Bayesian classifier can be formulated in its most general case as equation (3), which gives an intractable problem due to the high dimensionality of the fields $\boldsymbol{L}$ and $\boldsymbol{D}$,

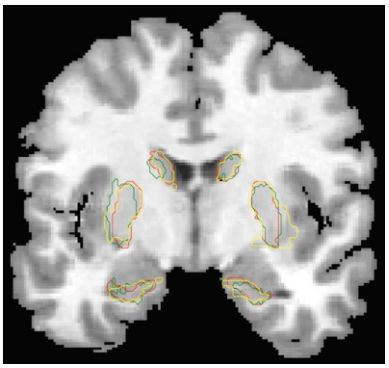

Fig. 1. The borders of the hippocampus, putamen, and caudate in the manually labeled (red), FreeSurfer (yellow) and MAP-QMRF (green) on a coronal slice.

$$P(\boldsymbol{l}|\boldsymbol{d}) \propto P(\boldsymbol{d}|\boldsymbol{l}) \times P(\boldsymbol{l}) \quad (3)$$

The traditional MAP-MRF framework uses the Markov-Gibbs equivalency to incorporate the neighboring labels information into the computation of the prior $P(\boldsymbol{l})$ and computes the likelihood under the conditional independency assumption by $P(\boldsymbol{d}|\boldsymbol{l}) = \prod_{i\in S} P(d_i|l_i)$ in which $P(d_i|l_i)$'s are simplified further by in class homogeneity assumption stated in equation (2). However, a different paradigm has been taken into account in the proposed MAP-QMRF framework. Here, both joint distributions $P(\boldsymbol{l})$ and $P(\boldsymbol{d}|\boldsymbol{l})$ are obtained under the definition of new causal Markov model QMRF. This means that not only will the neighboring voxels labels be taken into account in the classification process, but their intensities will be considered as well. Their joint distributions will be formulated in terms of two-dimensional neighboring distributions; therefore there will be no need for arbitrary potential functions or expectation maximization (EM) process to optimize it. The distribution of the first order homogeneous QMRF in terms of two dimensional local conditional distributions is given in [5]. The joint distribution of the first order inhomogeneous anisotropic QMRF is given by equation (4).

$$P(\boldsymbol{l}) = \prod_{i\in S} \prod_{l_j\in N_i} \prod_{(l_h,l_k)\in N_i'} \frac{\left[P(l_i,l_j)\right]^{1/2}}{P(l_i)\left[P(l_j)\right]^{1/4}[P(l_h,l_k)]^{1/8}} \quad (4)$$

where $N_i = \{l_i^u, l_i^d, l_i^l, l_i^r\}$ is the set of 4 nearest neighbor pixels of i and $N_i' = \{(l_i^u, l_i^l), (l_i^u, l_i^r), (l_i^d, l_i^l), (l_i^d, l_i^r)\}$, where l_i^u is the up, l_i^d is the down, l_i^l is the left, and l_i^r is the right neighbor of the random variable l_i. The derivation of equation (4) is similar to the one obtained for a homogeneous random field given in [5]; thus it is not repeated here. The likelihood probability $P(\boldsymbol{d}|\boldsymbol{l})$ is also formulated in terms of QMRF, which is given in equation (5).

$$P(\boldsymbol{d}|\boldsymbol{l}) = \prod_{i\in S}\prod_{l_j\in N_i}\prod_{(l_h,l_k)\in N_i'} \frac{\left[P\left((d_i,d_j)\middle|(l_i,l_j)\right)\right]^{1/2}}{P(d_i|l_i)\left[P(d_j|l_j)\right]^{1/4}\left[P((d_h,d_k)|(l_h,l_k))\right]^{1/8}} \quad (5)$$

where $\boldsymbol{d}$ is a realization of the random field $\boldsymbol{D}$ which is a sample of an intensity image. Equation (5) is simply derived from the extension of equation (4) to a vector random field in which each random variable is a vector if two random variables, $[d_i, l_i]$. All the probabilities in the right side of the equations (4) and (5) are estimated by a normalized joint histogram for different neighboring cliques. Solving equation (3) in its most general case is intractable due to the infinite number of the possibilities in realization of $\boldsymbol{D}$ and $\boldsymbol{L}$. Instead we employ an iterative local minimization method for finding the optimal solution and the simplest Bayesian classifier in equation (2) as the initializer. This initial segmentation is then sequentially updated at each location i by obtaining the label l_i, which maximizes the following conditional posteriori probability

$$P\left(l_i\middle|\boldsymbol{l}_{\{S-i\}},\boldsymbol{d}\right) \propto P(\boldsymbol{d}|\boldsymbol{l}) \times P\left(l_i\middle|\boldsymbol{l}_{N_i}\right) \quad (6)$$

where the prior probability is computable from equations (4) and by

$$P\left(l_i\middle|\boldsymbol{l}_{N_i}\right) = {P(\boldsymbol{l})}\Big/{\sum_{l_i\in\mathcal{L}} P(\boldsymbol{l}')} \quad (7)$$

where $\boldsymbol{l}'$ is the same configuration as $\boldsymbol{l}$ in all locations except i. Please note only the terms containing l_i needs to be recomputed in each iteration for the computation of $P(\boldsymbol{d}|\boldsymbol{l})$, and $P(\boldsymbol{l})$.

3. EXPERIMENTAL RESULTS

In this section, we use MAP-QMRF to perform the volumetric segmentation of human brain MR images; then we evaluate the results by comparing them to the manually labeled brains and computing the Dice overlap measure for every region. We train and assess the MAP-QMRF classifier with the same dataset using the jackknife validation method (systematically recomposing the statistic estimate leaving out one observation at a time from the sample set). We also compare the final results with the results of the FreeSurfer on the same images.

Training dataset is required in the proposed MAP-QMRF framework to estimate the two-dimensional distributions in equations (4). The brain images are selected from the open access series of imaging studies (OASIS) database [8] and the labeling is done by the ongoing labeling project at Neuromorphometrics Inc. (http://www.Neuromorphometrics.com/) where experts are manually labeling structural scans using a protocol that precisely specifies the borders of 144 neuroanatomical regions of interest. The original labels are converted to 24 subcortical labels: white matter (WM), gray matter (GM), hippocampus (Hp), amygdala (Am), putamen (Pu), pallidum (Pa), caudate (Ca), thalamus (Th), cerebellum white matter (CWM), cerebellum gray matter (CGM), and lateral ventricle (LV), on both hemisphere and also CSF, and brain stem (BS).

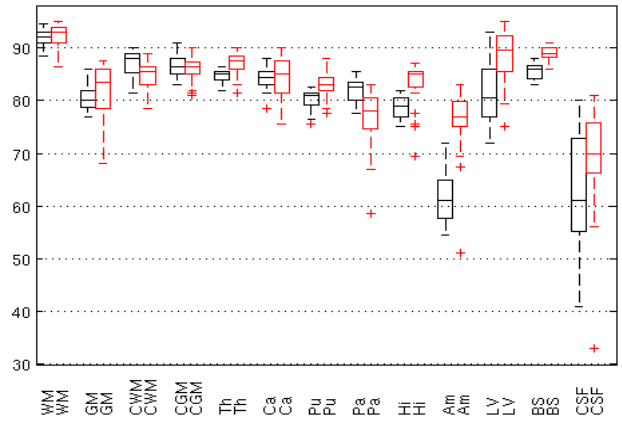

Fig. 2. Comparison of Dice overlap measure between MAP-OMRF (red) and FreeSurfer (black)

Pre-processing is done here to prepare the labeled and intensity images to be processed by the classifier. Since the final results are going to be compared with FreeSurfer, we use the same method as FreeSurfer to do bias field correction and intensity standardization described in [9]. Spatial normalization of the MR brain images is done by linear registration (12 degree of freedom) of the images to MNI152 atlas space.

Using the labeled and intensity images in standard space, MNI152, all the joint distribution in the right side of the equation (4) can be obtained at each voxel by their normalized histogram. Therefore, there is no need to deal with the Gibbs distribution, obtaining its clique potential functions and optimizing its parameters. We only have access to 20 labeled brain images at this time which is not enough to build the likelihood probability in the proposed MAP-QMRF framework. Therefore, only the prior of the classifier was modeled by QMRF and the likelihood was computed under the conditional independency assumption, equation (2). First the simplest method in equation (2) was employed to obtain the initializer. Then this initialization was fed into the iterative process in the proposed method to obtain the final result. From the training dataset, 19 images are used to build the prior based on QMRF with nearest neighborhood and one image is left out for testing the model. This process is repeated 20 times to get 20 labeled images. Fig. 3 shows the borders of the hippocampus, putamen, and caudate in the manually labeled (red), FreeSurfer labeled (yellow) and the output of the proposed method (green) on a sample coronal slice. The Dice overlap measures between the manually labeled image and the MAP-QMRF and FreeSurfer results are reported in Fig. 2 for 13 different neuroanatomical structures. On average, MAP-QMRF shows 1.8% increase in the segmentation accuracy over Dice overlap measure. Next we perform a

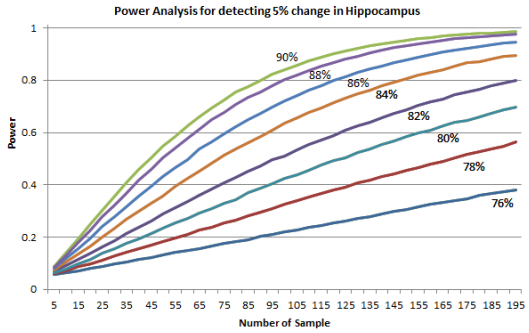

Fig. 3. Power analysis for detecting 5% reduction in the volume of hippocampus in human MR images

power analysis to show the effect of such increase in the accuracy of the segmentation in its practical applications.

4. POWER ANALYSIS

Power analysis is done here to show that even a small increase in the Dice overlap measure is crucial for detecting the change in brain neuroanatomical structures, and reducing the number of required subjects. To show the relationship between the segmentation accuracy and the required number of subjects, we performed the following simulation: 1) An accurately and manually delineated hippocampus volume is extracted from a single brain and saved as a separate binary image, 2) 5% shrinkage is applied to this hippocampus region to obtain a smaller version. 3) By manipulating the border voxels (inner and outer), we create 500 different hippocampus volumes which overall look like the original one but the Dice overlap between them is 76%. 4) In the same way, we created 500 different hippocampus volumes from the smaller version. 5) Five subjects' volumes are randomly selected from both groups and student's t-test is performed ($\alpha = .5$) to reject the null hypothesis (mean equality). 6) This is repeated 10^5 times and the ratio of the rejected times to accepted times of the null hypothesis is reported as the power for the five number of subjects. 7) The power curve is obtained by repeating this process for different number of subjects (from 5 to 200, with a step size of 5). 8) The entire process is repeated to obtain power curves for the overlap measures from 76% to 90% by 2% step size and the results are shown in Fig. 4. As shown in this figure, the power for detecting 5% change is low for overlap measures less than 82%, even for a high number of subjects (>200). Also, for 100 subjects, a 4% increase in Dice overlap (from 76% to 80%) doubles the chance of detecting the 5% change. On the other hand, for 80% chance of detection, the required number of subject drops from 200 to 150 with an increase of 2% in Dice overlap. These results clearly indicate that even a small improvement in the accuracy of the segmentation has a significant effect in its practical applications.

5. CONCLUSION

We have established a new MAP classifier using first order inhomogeneous anisotropic QMRF model. The new classifying framework was trained and assessed using 20 manually labeled human brain MR images using the jackknife validation method. The same images have been labeled using the FreeSurfer software package and the accuracy of the both methods is reported in compare to manual labels by Dice overlap measure. It is shown that on average MAP-QMRF outperforms FreeSurfer by 1.8% on Dice overlap. We also used power analysis to show that this improvement in accuracy of the segmentation may reduce the number of required samples up to 50 subjects for detecting 5% change in the volume of a hippocampal region.

6. REFERENCES

[1] Y. Zhang, M. Brady, and S. Smith, "Segmentation of brain MR images through a hidden Markov random field model and the expectation-maximization algorithm," *IEEE Transactions on Medical Imaging*, vol. 20, 2001, pp. 45-57.

[2] J. Ashburner and K.J. Friston, "Unified segmentation.," *NeuroImage*, vol. 26, pp. 839-51, 2005.

[3] B. Fischl, D. H Salat, E. Busa, M. Albert, M. Dieterich, and C. Haselgrove, "Whole brain segmentation: automated labeling of neuroanatomical structures in the human brain," *Neuron*, vol. 33, pp. 341-355, 2002.

[4] Z. Li Stan, *Markov random field modeling in image analysis* (3rd Ed.), Springer, 2009.

[5] Q.R. Razlighi, N. Kehtarnavaz, and A. Nosratinia, "Computation of image spatial entropy using quadrilateral Markov random field.," *IEEE transactions on image processing*, vol. 18, pp. 2629-39, 2009.

[6] R. de Boer, H. a Vrooman, M.A. Ikram, M.W. Vernooij, M.M.B. Breteler, A. van der Lugt, and W.J. Niessen, "Accuracy and reproducibility study of automatic MRI brain tissue segmentation methods.," *NeuroImage*, vol. 51, pp. 1047-56, 2010.

[7] F. Klauschen, A. Goldman, V. Barra, A. Meyer-Lindenberg, and A. Lundervold, "Evaluation of automated brain MR image segmentation and volumetry methods.," *Human Brain Mapping*, vol. 30, pp. 1310-1327, 2009.

[8] D.S. Marcus, T.H. Wang, J. Parker, J.G. Csernansky, J.C. Morris, and R.L. Buckner, "Open Access Series of Imaging Studies (OASIS): cross-sectional MRI data in young, middle aged, nondemented, and demented older adults.," *Journal of cognitive neuroscience*, vol. 19, pp. 1498-507, 2007.

[9] X. Han and B. Fischl, "Atlas renormalization for improved brain MR image segmentation across scanner platforms," *IEEE Transactions on Medical Imaging*, vol. 26, pp. 479-486, 2007.